RSC Advances

PAPER

View Article Online
View Journal | View Issue

Cite this: *RSC Adv.*, 2014, **4**, 50188

Electron transport *via* phenyl–perfluorophenyl interaction in crystals of fluorine-substituted dibenzalacetones

Ling Liu, Guochun Yang,* Yun Geng, Yong Wu and Zhongmin Su*

Received 27th August 2014
Accepted 25th September 2014

DOI: 10.1039/c4ra09323b

www.rsc.org/advances

Although substitution with fluorine creates stability in organic electronic materials by altering the molecular crystal packing, the charge transport properties of the materials are significantly affected. Phenyl–perfluorophenyl (π–π_F) interaction is a unique intermolecular interaction formed between electropositive perfluorophenyl and electronegative non-fluorinated phenyl, and may have a different charge transport as compared to the π–π interaction formed between ordinary phenyl rings. Three crystals with both π–π_F interaction and intermolecular hydrogen bonding interaction were chosen to study the relationship between intermolecular interactions and their charge transport properties in both the band-like model and the hopping model. In contrast to ordinary π–π interaction, which has been reported to be mainly responsible for hole transport, the π–π_F interaction is mainly responsible for electron transport. Thus, intermolecular π–π_F interaction is an effective packing style to realize the n-type charge carrier. In summary, C–H···F interactions are mainly responsible for electron transport while the C–H···O interaction is responsible for hole transport.

1 Introduction

The development of organic electronic materials has always been an active area of research since their discovery in the 1950s. Highly conductive polyacetylene was discovered in the mid-1970s by Shirakawa, MacDiarmid, and Heeger,[1,2] and was rapidly developed in the following decades with remarkable achievements. Various organic materials with outstanding properties were either designed or synthetized. They are inexpensive, lightweight, flexible, have a large surface area, and can be widely used in a variety of applications such as organic light emitting diodes (OLEDs),[3,4] organic field effect transistors (OFETs),[5,6] organic photovoltaic cells (OPVs),[7] and sensors.[8] However, despite the advantages, there are still several disadvantages when compared with traditional semiconductor materials, such as low mobility and instability due to the complexity of their molecular structures, varied packing motifs of their crystal structures, uncontrollable intermolecular interactions, and lack of knowledge regarding structure–property relationships, which have always been the main challenges in this field.[9] Thus, a complete understanding of the fundamental chemical and physical aspects behind the structural design to achieve better charge transport properties and stability is desired.

Fluorine is an important element that is involved in many parts of our daily life, from health care to the alternative energy sector.[10,11] Due to its electron-withdrawing characteristic, it is considered to be one of the potential substitutions that can solve the instability problem in organic electronic materials by altering the molecular packing in their crystals; however, this can significantly affect the charge transport properties of the materials.[9–13] A number of fluorine-substituted compounds with different intermolecular interactions have been synthesized; however, they have different charge transport properties. For example, perfluoropentacene is an n-type semiconductor with an electron mobility of 0.11 cm^2 (V^{-1} s^{-1}).[14] The compound 2,2′-bis(4-trifluoromethylphenyl)-5,5′-bithiazole, which was synthesized by Yamashita and coworkers with an electron mobility as high as 1.83 cm^2 (V^{-1} s^{-1}), is considered to have the highest reported electron mobility value for halogen n-type semiconductors.[9,15] The α polymorph of *p*-$CF_3C_6H_4$-substituted 2,6′-bi(thieno[2,3-c]thiophene), synthesized by Yamaguchi and coworkers, is reported to have a hole mobility up to 4.0 cm^2 (V^{-1} s^{-1}) along its longer axis and a mobility of 1.3 cm^2 (V^{-1} s^{-1}) as an isotropic value.[16]

In order to understand microscopic structures and behaviors that molecular or supramolecular systems acquire under certain conditions, it is imperative to understand the rules that govern weak intermolecular interactions such as hydrogen bonding and π–π interactions. As many studies have shown, intermolecular interaction plays a significant role in photophysics, photochemistry, and photobiology, as well as photoinduced electron transfer and charge transportation.[17–22] Generally, compounds with fluorine substituents undergo interactions that are classified as π–π_F, C–F···H, F···F, or

Institute of Functional Material Chemistry, Faculty of Chemistry, Northeast Normal University, Changchun, 130024 Jilin, China. E-mail: yanggc468@nenu.edu.cn

C–F$\cdots\pi_F$ interactions. The π–π_F interaction is a unique intermolecular interaction, stabilized by coulombic and dispersion forces, with a stabilization energy of approximately 20–25 kJ mol^{-1}.[23] Unlike π–π interactions formed between non-fluorinated phenyls, this type of interaction is formed between the electropositive perfluorophenyl and electronegative non-fluorinated phenyl.[24–26] With a centre-to-centre separation of 3.4–4.8 Å (ref. 23 and 27) and inter-ring angles of up to 20°,[11] the interaction offers considerable flexibility in forming crystal structures.

There is evidence that this kind of interaction could, to some extent, affect packing motifs, with the 1 : 1 mixture co-crystal of benzene/hexafluorobenzene forming a face-to-face structure in contrast to the edge-to-face structure formed by either of the molecules alone.[28,29] The angles of the C–H$\cdots$F interaction can range from 70° to 180° with a distance of 2.67 Å to 2.9 Å.[10] It is a much weaker intermolecular interaction compared to typical H-bonds with acceptors such as oxygen or nitrogen, and it has been suggested by Dunitz and Taylor that the different energies of the competing orbitals can be influenced by the electron delocalization of the molecules.[30] Yet such weak interactions still can influence the structure and properties of organic fluorine compounds in the same way as C–H$\cdots$O and C–H$\cdots$N interactions.[31–33] As to the F$\cdots$F interaction, whether this contact is steady or simply a consequence of the molecules being packed so closely in the crystal is still surrounded by controversy,[11,34–39] because such interactions are rare and weak. However, it has been reported that in some cases, the F$\cdots$F contacts could either drive or at least affect crystal packing.[38,39] Finding C–F$\cdots\pi_F$ interaction in perfluorinated compounds is not rare, as it has been found in fluorinated benzophenones, *N*-phenylmaleimides, and phthalimides.[35,36] The electron density distribution in a perfluorinated aromatic ring is inversed to a common aromatic system, and it can form more stable contacts with the C–F group. However, this interaction is also considered to be primarily determined by close packing.[10,11]

In this work, we have chosen molecules **1**, **2**, and **3** and their corresponding crystals **a**, **b** and **c**, synthesized by Anke Schwarzer and Edwin Weber,[40] to study the relationship between charge transport and intermolecular interactions, especially for the π–π_F interaction. Molecules **1**, **2**, and **3** are decafluoro (1,5-bis-(2,3,4,5,6-pentafluorophenyl)penta-1,4-dien-3-one), pentafluoro (1-phenyl-5-(2,3,4,5,6-pentafluorophenyl)penta-1,4-dien-3-one), and nonfluoro (1,5-diphenyl-1,4-pentadien-3-one) substituted dibenzalacetone, respectively. Crystals **a** and **b** each contain only one kind of molecule, which are molecule **1** for crystal **a** and molecule **2** for crystal **b**, while crystal **c** is a 1 : 1 mixture of the decafluorinated derivative **1** and the nonfluorinated parent **3**. These crystals contain some of the intermolecular interactions introduced above, and two of the three have π–π_F interaction between molecules, which offers us a good opportunity to study the relationship between these intermolecular π–π_F interactions and their charge transport properties. The results will be helpful for further understanding the charge transport property for these types of compounds and provide data that can be utilized for material design.

2 Theoretical methodology

The band-like model and hopping model are widely used in calculations of the charge transport mechanism in organic semiconductor materials. In a standard band-theory model, given by the gradient of the band energy in *k*-space, the group velocity $v(k)$ of the delocalized electron or hole wave can be expressed as.

$$\vec{v}(k) = \nabla k E(k)/h \quad (1)$$

where $E(k)$ is the band structure of the system, k is the wave vector, and h is the Planck constant with $\hbar = h/2\pi$. As presented in eqn (1), the charge velocity $\vec{v}(k)$ is in proportion to the slope of $E(k)$. Generally, the larger the band dispersion, the higher the mobility.

The charge transport mechanism of the hopping model can be described as a nonadiabatic electron-transfer reaction from a charged molecule to an adjacent neutral one involving the self-exchange charge. The rate, k, of charge transfer between neighboring molecules can be expressed by the standard Marcus equation[41,42]

$$k = \frac{4\pi^2}{h}\frac{1}{\sqrt{4\pi\lambda k_B T}}V^2 \exp\left(-\frac{\lambda}{4k_B T}\right) \quad (2)$$

where λ, V, and T are the reorganization energy, the transfer integral, and the temperature of the system, respectively, while h and k_B are the Planck and Boltzmann constants, respectively. Usually, a larger transfer integral will lead to a larger transfer rate.

In this work, both of these models were used to describe the transport properties of the studied crystals. Electronic band structure calculation was performed using a density functional theory (DFT) method implemented in the Vienna *Ab initio* Simulation Package (VASP)[43,44] with Perdew–Burke–Emzerhof (PBE) for the exchange correlation functionals and a plane-wave basis set with an energy cut-off of 400 eV.[45,46] For the crystal structure of **a**, **b**, and **c**, the space groups were $P2_1/c$, $P2_1/c$, and $P\bar{1}$, respectively; the *K*-grids were 6 × 2 × 2, 6 × 8 × 2, and 6 × 4 × 2, respectively. The Monkhorst–Pack scheme was used to sample the *K*-grids in the Brillouin zone.

The hole or electronic coupling (charge transfer integral) was calculated with the PW91 functional Slater-type triple-ζ plus polarization (TZP) basis set for all atoms through the Amsterdam Density Functional (ADF) package.[47–49] The Γ point wave function calculations were performed through Dmol3 within the Material Studio[50,51] software package with the generalized gradient approximation (GGA) in Perdew–Burke–Ernzerhof (PBE) form and the all-electron double numerical basis set with polarized function (DNP basis set).[52]

3 Results and discussion

3.1 Geometric structure

The structures of molecules **1**, **2**, and **3**, which are decafluoro-, pentafluoro-, and nonfluoro-substituted dibenzalacetone, respectively, are shown in Fig. 1. The crystal structures **a**, **b**, and

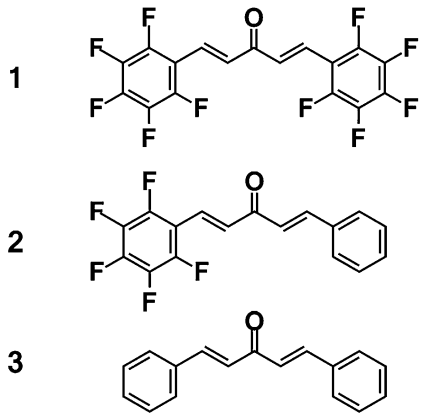

Fig. 1 The molecular structures of **1**, **2**, and **3**.

c, together with the main intermolecular interactions in these crystals, are shown in Fig. 2. The packing motifs of crystals **a**, **b**, and **c** are a herringbone packing motif without π–π overlap, slipped π-stacking, and lamellar motif, respectively. All of these molecules exhibit planar molecular structures in the studied crystals. Here, we only introduce the intermolecular interactions that have been proven to have contributed to charge transport in these crystals because our interest lies in the charge transport abilities of these materials.

Crystals **a** and **b** only contain one kind of molecule, *i.e.*, molecule **1** for crystal **a** and molecule **2** for crystal **b**. Crystal **a** is the only crystal of the three that does not exhibit π–π_F interaction, as there are no overlaps between molecular layers. There are simply hydrogen bonding interactions in crystal **a**, which are C–H···O and C–H···F interactions, stretching parallel to the molecular layer, with distances of 2.6 and 2.5 Å, respectively. In crystal **b**, the π–π_F interaction is in the direction of the *a*-axis with perpendicular distances between the interacting ring planes of approximately 3.5 Å, while C–H···O and C–H···F interactions in this crystal stretch parallel to the *ab* plane. Distances between the interacting atoms are from 2.5 to 2.7 Å for C–H···O and from 2.5 to 2.6 Å for C–H···F.

Crystal **c** is a 1 : 1 mixture of the decafluorinated derivative **1** and the nonfluorinated parent **3**. The π–π_F interaction in this crystal is in the same direction as that of crystal **b**, which is along the *a*-axis, with perpendicular distances between the interacting ring planes of approximately 3.4 Å, while the C–H···F interactions in this crystal, unlike the others, stretch along two different directions. One of the directions is along the *b*-axis together with C–H···O interactions. The distances of these interactions are 2.5 Å for C–H···F and 2.4 Å for C–H···O, while the other direction with only C–H···F interaction is along the *c*-axis with a distance of interaction from 2.6 Å.

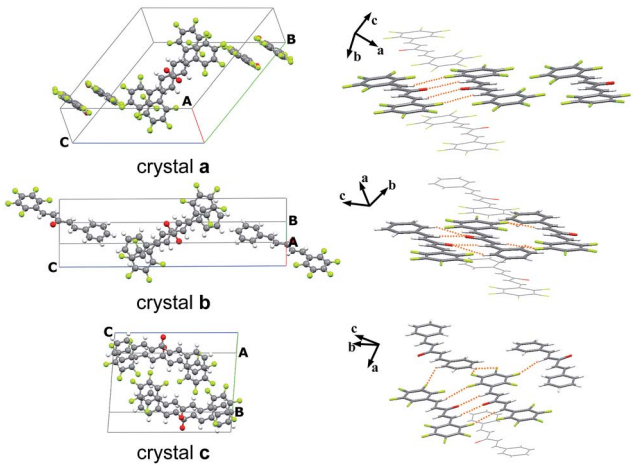

Fig. 2 The crystal structures and the main intermolecular interactions of **a**, **b**, and **c**. The intermolecular hydrogen bonding interactions are connected by dashed orange lines.

3.2 Band structure

The appearances of bands, dispersive or flat, are reflections of the anisotropy in the charge transports of the crystal. Generally, a stronger dispersion of the band indicates that the crystal possesses a larger carrier mobility. With the help of first principles calculations, we have calculated the band structures along the high symmetry directions of these crystals, and the results are shown in Fig. 3. Crystal **a** is a direct band gap semiconductor with a band gap of 1.98 eV, due to the maxima of its valence band (VB) and conductive band (CB) being at the Γ point. Crystals **b** and **c** are indirect band gap semiconductors with band gaps of 2.20 and 1.84 eV, respectively, and valence band maximums at the *X* and Γ points, respectively, while the conduction band minimum is at the Y point for both.

The calculated larger bandwidths in the VB and CB along with their corresponding directions in the first Brillouin zone are listed in Table 1. A comparison of the bandwidths of the VB and CB shows that crystals **a** and **c** are ambipolar and electron transport materials, respectively. The band dispersion in crystal **b** shows anisotropy between two directions that are almost vertical with each other, resulting in electron and ambipolar charge transport, respectively, in the two directions. There are no π–π_F interactions in crystal **a**; only C–H···O and C–H···F hydrogen bonding interactions occur, which contribute to charge transport. The crystal structure analysis indicates that the two hydrogen bonding interactions stretch parallel to the molecular layer, corresponding to direction $\Gamma \rightarrow E$ in the first Brillouin zone. The bandwidth of the VB and CB in this direction are 0.060 and 0.051 eV, respectively, which suggests similar but not identical charge transport abilities for both hole and electron.

Crystal **b** exhibits π–π_F interaction in high symmetry direction $\Gamma \rightarrow X$ in the first Brillouin zone, corresponding to the *a*-axis in real space. This kind of interaction is mainly responsible for electron transport, due to the bandwidth (0.029 eV) in the CB being larger than that (0.003 eV) in the VB, which is in contrast to π–π interaction forms between ordinary phenyl rings that have been reported as mainly responsible for hole transport.[53–56] The hydrogen bonding interactions C–H···O and C–H···F in this crystal coexist in the same direction parallel to the molecular layer, corresponding to direction $\Gamma \rightarrow E$, and the evolution of

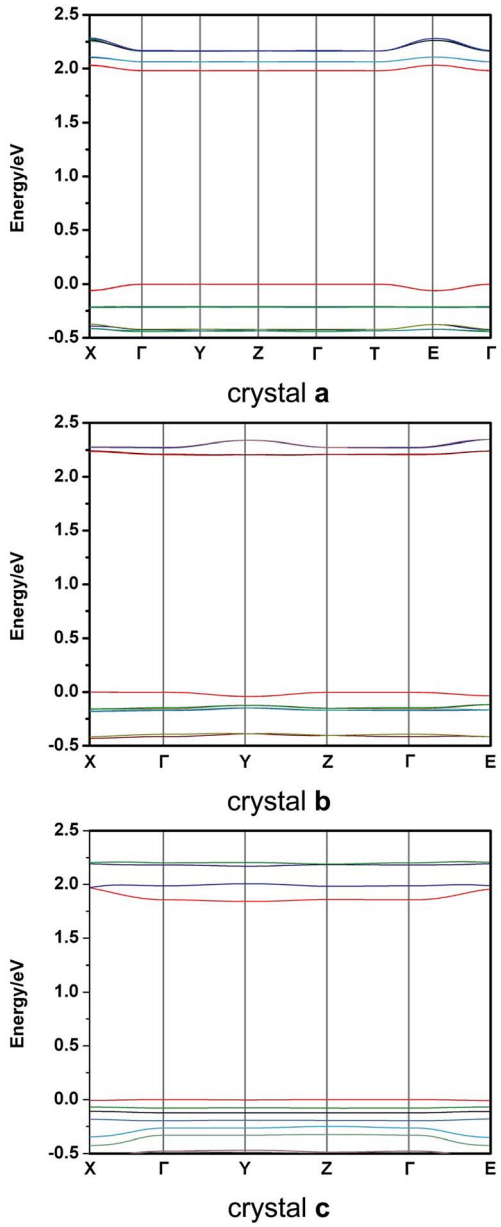

Fig. 3 The band structures of **a**, **b**, and **c**. High symmetry *k*-points in the first Brillouin zone are $\Gamma = (0, 0, 0)$, $X = (0.5, 0, 0)$, $Y = (0, 0.5, 0)$, $Z = (0, 0, 0.5)$, $T = (0, 0.5, 0.5)$, and $E = (0.5, 0.5, 0.5)$.

identical bandwidths of the VB and CB, which are 0.032 and 0.035 eV, respectively, suggests equal charge transport abilities in both hole and electron.

For crystal **c**, the π–π_F interaction also stretches along the *a*-axis in real space in the same manner as crystal **b**, and corresponds to high symmetry direction $\Gamma \rightarrow X$ in the first Brillouin zone. Bandwidth (0.111 eV) in the CB that is significantly larger than that (0.008 eV) in the VB indicates that π–π_F interaction in crystal **c** is mainly responsible for electron transport. The hydrogen bonding interactions C–H···O and C–H···F in this crystal also coexist in the same direction, which is along the *b*-axis in real space, corresponding to high symmetry direction $\Gamma \rightarrow Y$ in the first Brillouin zone. However, bandwidths in this crystal do not show much dispersion, unlike what was found in crystals **a** and **b**.

Table 1 The largest bandwidths (in eV) in the VB and CB of **a**, **b**, and **c** along high symmetry directions

	Directions	Interactions	VB (eV)	CB (eV)
a	ΓE	C–H···F and C–H···O	0.060	0.051
	ΓT	—	—	0.001
b	ΓX	π–π_F	0.003	0.029
	ΓE	C–H···F and C–H···O	0.032	0.035
c	ΓZ	C–H···F	0.003	0.018
	ΓY	C–H···F and C–H···O	0.003	0.015
	ΓX	π–π_F	0.008	0.111

The electronic band structure calculations indicate that π–π_F interaction is mainly responsible for electron transport, which is greatly different from the typical π–π interaction. This finding can be applied to situations where the performance of n-type carrier transport may be desired, which is far behind that of p-type carrier transport.[9] Further calculations should be performed before we can finally determine how C–H···O and C–H···F interactions function in charge transport.

3.3 Transfer integral

In addition to the band model, we also calculated the transfer integrals of these systems using the hopping model. The transfer integrals are an important parameter when assessing charge transport properties of organic semiconductor material. They are the separation of the highest occupied molecular orbital (HOMO) and the lowest unoccupied molecular orbital (LUMO), which requires a large π-overlap area between neighboring molecules.[57] Since it is calculated only between neighboring molecules, we are expecting a separation of each kind of intermolecular interaction, which should allow us to precisely determine how each kind of interaction affects charge transport. In general, a larger transfer integral is required in order to achieve a better charge mobility.

The hole and electron transfer integrals were calculated with the PW91 functional Slater-type TZP basis set for all atoms through the ADF package. The pathways corresponding to intermolecular interactions are shown in Fig. 4. The calculated results together with the directions in the first Brillouin zone of each selected pathway are listed in Table 2.

A comparison of bandwidths and transfer integrals in each direction indicates that the results generally fit with each other and have provided evidence to identify the mechanism for each kind of intermolecular interaction during charge transport. Pathways 2 and 4 in crystal **b** together with pathway 4 in crystal **c** all contain π–π_F interaction. For each of these pathways, the electron transfer integrals tend to be larger than those of holes. Therefore, the π–π_F interaction is mainly responsible for electron transport.

The hydrogen bonding interactions C–H···O and C–H···F in these crystals are not as complex as the π–π_F interaction, which stands apart from other types of interactions, because the

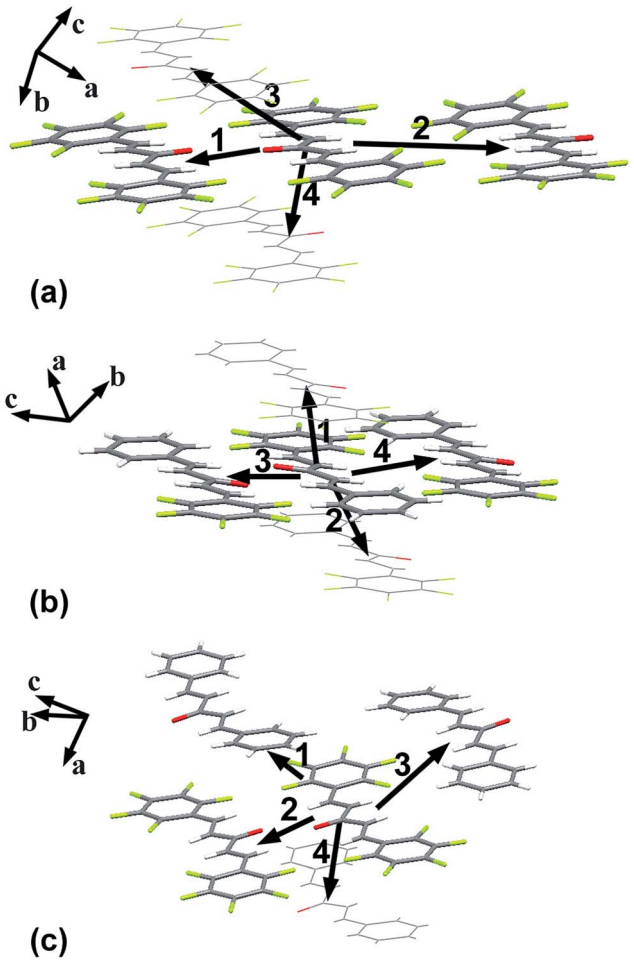

Fig. 4 The pathways of the charge transfer integral corresponding to intermolecular interactions in crystals **a**, **b**, and **c**.

Table 2 Hole (t_h) and electron (t_e) transfer integrals of **a**, **b**, and **c** in the pathways along high symmetry directions

	Directions	Interactions	Pathways	t_h (meV)	t_e (meV)
a	ΓE	C–H···F and C–H···O	1	83.88	37.69
		C–H···F	2	0.30	1.09
	ΓT	—	3	3.22	25.51
			4	23.14	28.90
b	ΓX	π–π_F	1	22.68	31.40
			2	2.15	11.00
	ΓE	C–H···F and C–H···O	3	57.65	19.56
		C–H···F	4	0.48	0.23
c	ΓZ	C–H···F	1	0.10	0.07
	ΓY	C–H···F and C–H···O	2	100.02	39.93
		C–H···F	3	10.78	45.13
	ΓX	π–π_F	4	0.45	45.35

hydrogen bonding interactions are stretching in the same direction in the first Brillouin zone and acting between the same pair of molecules in most circumstances. However, it is still possible for us to find two pathways, although not in the same crystal, which contain C–H···O or C–H···F, respectively. Pathway 1 in crystal **b** contains only the C–H···O interaction, and its hole transfer integral (57.65 meV) is apparently larger than its electron transfer integral (19.56 meV). Yet pathway 1 in crystal **c**, which contains only the C–H···F interaction, has a rather small hole transfer integral (10.78 meV) as compared to its electron transfer integral (45.13 meV). The C–H···O interaction is mainly responsible for hole transport, while the C–H···F interaction is mainly responsible for electron transport. The other pathways such as pathway 2 in crystal **a** and pathway 3 in crystal **c** also support this conclusion due to their great transfer integrals for both hole and electron transport, as C–H···O and C–H···F interactions coexist. Moreover, the larger hole transport integrals in the pathways are responsible for larger bandwidths in the VB than the CB of the $\Gamma \rightarrow E$ direction in crystal **a**, which indicates stronger C–H···O interaction than C–H···F interaction in this direction.

3.4 Γ point wave functions

In general, there is a close relationship between the charge transport and distribution of frontier molecular orbitals. The wave functions of the band-edge state at the Γ point are equivalent to the frontier molecular orbitals, namely, the HOMO for the hole and LUMO for the electron. The calculated Γ point wave functions are shown in Fig. 5, which illustrates that the three crystals have almost identical electron cloud distributions in either their HOMO or LUMO despite the different packing motifs. The distributions of the HOMO in these crystals are all shaped like a butterfly and localized around the C=O bond, well attached to neighbouring molecules, which confirms the previous conclusion that the C–H···O interaction is mainly responsible for hole transport. The LUMO of crystals **b** and **c** all show good distributions on their phenyl and pentafluorophenyl rings, which also confirms the previous conclusion that the π–π_F interaction is mainly responsible for electron transport.

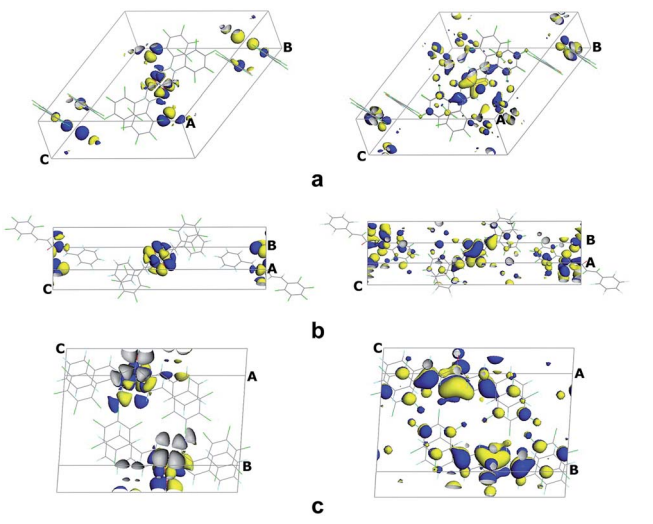

Fig. 5 Γ point wave functions of **a**, **b**, and **c**. HOMO (left), LUMO (right).

4. Conclusions

The analysis of the molecular structures and the calculated results for these crystals indicate that crystals **a** and **c** are ambipolar and electron transport materials, respectively. The band dispersion in crystal **b** indicates anisotropy between two directions and results in electron and ambipolar charge transport in two directions. In contrast to the π–π interaction formed between ordinary phenyl rings for hole transport, the π–π_F interaction was mainly responsible for electron transport in these crystals, which provides a good opportunity to realize an n-type charge carrier. Hydrogen bonding interactions C–H···F and C–H···O also affect charge transport in different ways. Specifically, C–H···F interactions are mainly responsible for electron transport, and the C–H···O interaction governs hole transport. These results will assist with further understanding of the charge transport property of these types of compounds and provide data that can be utilized for material design.

Acknowledgements

The authors gratefully acknowledge the financial support from the National Natural Science Foundation of China (21273030 and 21203019), the Science and Technology Development Project Foundation of Jilin Province (20090146), and the project sponsored by the Scientific Research Foundation for Returned Overseas Chinese Scholars, State Education Ministry.

References

1 C. Chiang, C. Fincher, Y. Park, A. Heeger, H. Shirakawa, E. Louis, S. Gau and A. G. MacDiarmid, *Phys. Rev. Lett.*, 1977, **39**, 1098–1101.
2 H. Shirakawa, E. J. Louis, A. G. MacDiarmid, C. K. Chiang and A. J. Heeger, *J. Chem. Soc., Chem. Commun.*, 1977, **16**, 578–580.
3 M. S. Park and J. Y. Lee, *Chem. Mater.*, 2011, **23**, 4338–4343.
4 N. Lin, J. Qiao, L. Duan, H. Li, L. Wang and Y. Qiu, *J. Phys. Chem. C*, 2012, **116**, 19451–19457.
5 D. T. Chase, A. G. Fix, S. J. Kang, B. D. Rose, C. D. Weber, Y. Zhong, L. N. Zakharov, M. C. Lonergan, C. Nuckolls and M. M. Haley, *J. Am. Chem. Soc.*, 2012, **134**, 10349–10352.
6 G. Generali, F. Dinelli, R. Capelli, S. Toffanin, F. di Maria, M. Gazzano, G. Barbarella and M. Muccini, *J. Phys. Chem. C*, 2011, **115**, 23164–23169.
7 I. Osaka, T. Abe, M. Shimawaki, T. Koganezawa and K. Takimiya, *ACS Macro Lett.*, 2012, **1**, 437–440.
8 L. Torsi, M. Magliulo, K. Manoli and G. Palazzo, *Chem. Soc. Rev.*, 2013, **42**, 8612–8628.
9 C. Wang, H. Dong, W. Hu, Y. Liu and D. Zhu, *Chem. Rev.*, 2012, **112**, 2208–2267.
10 K. Reichenbacher, H. I. Suss and J. Hulliger, *Chem. Soc. Rev.*, 2005, **34**, 22–30.
11 R. Berger, G. Resnati, P. Metrangolo, E. Weber and J. Hulliger, *Chem. Soc. Rev.*, 2011, **40**, 3496–3508.
12 C. Wang, H. Dong, H. Li, H. Zhao, Q. Meng and W. Hu, *Cryst. Growth Des.*, 2010, **10**, 4155–4160.
13 S. B. Heidenhain, Y. Sakamoto, T. Suzuki, A. Miura, H. Fujikawa, T. Mori, S. Tokito and Y. Taga, *J. Am. Chem. Soc.*, 2000, **122**, 10240–10241.
14 Y. Sakamoto, T. Suzuki, M. Kobayashi, Y. Gao, Y. Fukai, Y. Inoue, F. Sato and S. Tokito, *J. Am. Chem. Soc.*, 2004, **126**, 8138–8140.
15 S. Ando, R. Murakami, J.-i. Nishida, H. Tada, Y. Inoue, S. Tokito and Y. Yamashita, *J. Am. Chem. Soc.*, 2005, **127**, 14996–14997.
16 A. Fukazawa, D. Kishi, Y. Tanaka, S. Seki and S. Yamaguchi, *Angew. Chem., Int. Ed.*, 2013, **52**, 12091–12095.
17 K.-L. Han and G.-J. Zhao, *Hydrogen Bonding and Transfer in the Excited State*, John Wiley & Sons, Ltd, Chichester, UK, 2010DOI: 10.1002/9780470669143.
18 Y.-D. Wu, W. Han, D.-P. Wang, Y. Gao and Y.-L. Zhao, *Acc. Chem. Res.*, 2008, **41**, 1418–1427.
19 A. J. Alexander and R. N. Zare, *Acc. Chem. Res.*, 2000, **33**, 199–205.
20 G.-J. Zhao and K.-L. Han, *J. Phys. Chem. A*, 2009, **113**, 14329–14335.
21 G.-J. Zhao, J.-Y. Liu, L.-C. Zhou and K.-L. Han, *J. Phys. Chem. B*, 2007, **111**, 8940–8945.
22 G.-J. Zhao and K.-L. Han, *Acc. Chem. Res.*, 2012, **45**, 404–413.
23 S. Bacchi, M. Benaglia, F. Cozzi, F. Demartin, G. Filippini and A. Gavezzotti, *Chem.–Eur. J.*, 2006, **12**, 3538–3546.
24 S. E. Wheeler and K. N. Houk, *J. Am. Chem. Soc.*, 2008, **130**, 10854–10855.
25 S. E. Wheeler and K. N. Houk, *J. Chem. Theory Comput.*, 2009, **5**, 2301–2312.
26 C. J. Pace and J. Gao, *Acc. Chem. Res.*, 2012, **46**, 907–915.
27 A. S. Batsanov, I. A. I. Mkhalid and T. B. Marder, *Acta Crystallogr., Sect. E: Struct. Rep. Online*, 2007, **63**, o1196–o1198.
28 C. R. Patrick and G. S. Prosser, *Nature*, 1960, **187**, 1021.
29 G. W. Coates, A. R. Dunn, L. M. Henling, J. W. Ziller, E. B. Lobkovsky and R. H. Grubbs, *J. Am. Chem. Soc.*, 1998, **120**, 3641–3649.
30 J. D. Dunitz and R. Taylor, *Chem.–Eur. J.*, 1997, **3**, 89–98.
31 V. R. Thalladi, H.-C. Weiss, D. Bläser, R. Boese, A. Nangia and G. R. Desiraju, *J. Am. Chem. Soc.*, 1998, **120**, 8702–8710.
32 D. Chopra and T. N. G. Row, *CrystEngComm*, 2011, **13**, 2175–2186.
33 D. Chopra, *Cryst. Growth Des.*, 2011, **12**, 541–546.
34 A. Schwarzer, P. Bombicz and E. Weber, *J. Fluorine Chem.*, 2010, **131**, 345–356.
35 A. Schwarzer, W. Seichter, E. Weber, H. Stoeckli-Evans, M. Losada and J. Hulliger, *CrystEngComm*, 2004, **6**, 567–572.
36 A. Schwarzer and E. Weber, *Cryst. Growth Des.*, 2008, **8**, 2862–2874.
37 G. Asensio, M. Medio-Simon, P. Alemán and C. R. de Arellano, *Cryst. Growth Des.*, 2006, **6**, 2769–2778.
38 R. Bayón, S. Coco and P. Espinet, *Chem.–Eur. J.*, 2005, **11**, 1079–1085.
39 R. Mariaca, N.-R. Behrnd, P. Eggli, H. Stoeckli-Evans and J. Hulliger, *CrystEngComm*, 2006, **8**, 222–232.
40 A. Schwarzer and E. Weber, *Cryst. Growth Des.*, 2014, **14**, 2335–2342.

41 M. C. R. Delgado, K. R. Pigg, D. A. da Silva Filho, N. E. Gruhn, Y. Sakamoto, T. Suzuki, R. M. Osuna, J. Casado, V. Hernández, J. T. L. Navarrete, N. G. Martinelli, J. Cornil, R. S. Sánchez-Carrera, V. Coropceanu and J.-L. Brédas, *J. Am. Chem. Soc.*, 2009, **131**, 1502–1512.
42 R. S. Sánchez-Carrera, S. A. Odom, T. L. Kinnibrugh, T. Sajoto, E.-G. Kim, T. V. Timofeeva, S. Barlow, V. Coropceanu, S. R. Marder and J.-L. Brédas, *J. Phys. Chem. B*, 2009, **114**, 749–755.
43 J. Hafner, *J. Comput. Chem.*, 2008, **29**, 2044–2078.
44 E. F. C. Byrd, G. E. Scuseria and C. F. Chabalowski, *J. Phys. Chem. B*, 2004, **108**, 13100–13106.
45 G. Kresse and J. Furthmüller, *Phys. Rev. B: Condens. Matter Mater. Phys.*, 1996, **54**, 11169–11186.
46 G. Kresse and J. Hafner, *Phys. Rev. B: Condens. Matter Mater. Phys.*, 1993, **48**, 13115–13118.
47 G. Te Velde, F. M. Bickelhaupt, E. J. Baerends, C. F. Guerra, S. J. van Gisbergen, J. G. Snijders and T. Ziegler, *J. Comput. Chem.*, 2001, **22**, 931–967.
48 C. F. Guerra, J. Snijders, G. Te Velde and E. Baerends, *Theor. Chem. Acc.*, 1998, **99**, 391–403.
49 E. Baerends, J. Autschbach, A. Bérces, C. Bo, P. Boerrigter, L. Cavallo, D. Chong, L. Deng, R. Dickson and D. Ellis, *Instruction Manual of the Amsterdam Density Functional (ADF) Package*, SCM, Amsterdam, The Netherlands, 2012.
50 M.-Q. Long, L. Tang, D. Wang, L. Wang and Z. Shuai, *J. Am. Chem. Soc.*, 2009, **131**, 17728–17729.
51 N. L. Janaki, B. Priyanka, A. Thomas and K. Bhanuprakash, *J. Phys. Chem. C*, 2012, **116**, 22663–22674.
52 F. Yu, S.-X. Wu, Y. Geng, G.-C. Yang and Z.-M. Su, *Theor. Chem. Acc.*, 2010, **127**, 735–742.
53 Y. Y. Lin, D. J. Gundlach, S. F. Nelson and T. N. Jackson, *IEEE Electron Device Lett.*, 1997, **18**, 606–608.
54 T. W. Kelley, D. V. Muyres, P. F. Baude, T. P. Smith and T. D. Jones, *Mater. Res. Soc. Symp. Proc.*, 2003, **771**, 169–179.
55 L. Liu, G. Yang, X. Tang, Y. Geng, Y. Wu and Z. Su, *J. Mol. Graphics Modell.*, 2014, **51**, 79–85.
56 L. Liu, G. Yang, Y. Duan, Y. Geng, Y. Wu and Z. Su, *Org. Electron.*, 2014, **15**, 1896–1905.
57 J. L. Brédas, J. P. Calbert, D. A. da Silva Filho and J. Cornil, *Proc. Natl. Acad. Sci. U. S. A.*, 2002, **99**, 5804–5809.